JGR Oceans

Key Points:
- PGW is characterized by high spatiotemporal variability in its properties and transport that impacts the variability of the upper OMZ
- Oxygen contribution from PGW to the Arabian Sea OMZ is resolved for the first time as 1.3 Tmol yr^{-1}
- Intermittent shear-driven mixing at the PGW bottom boundary amplifies ventilation of the OMZ by salt fingering 14% of the time

Ventilation of the Arabian Sea Oxygen Minimum Zone by Persian Gulf Water

Estel Font[1], **Sebastiaan Swart[1,2]**, **Gerd Bruss[3]**, **Peter M. F. Sheehan[4]**, **Karen J. Heywood[4]**, and **Bastien Y. Queste[1]**

[1]Department of Marine Sciences, University of Gothenburg, Gothenburg, Sweden, [2]Department of Oceanography, University of Cape Town, Rondebosch, South Africa, [3]Department of Marine Science and Fisheries, Sultan Qaboos University, Muscat, Oman, [4]Centre for Ocean and Atmospheric Sciences, School of Environmental Science, University of East Anglia, Norwich, UK

Abstract Dense overflows from marginal seas are critical pathways of oxygen supply to the Arabian Sea oxygen minimum zone (OMZ), yet these remain inadequately understood. Climate models struggle to accurately reproduce the observed extent and intensity of the Arabian Sea OMZ due to their limited ability to capture processes smaller than their grid scale, such as dense overflows. Multi-month repeated sections by underwater gliders off the coast of Oman resolve the contribution of dense Persian Gulf Water (PGW) outflow to oxygen supply within the Arabian Sea OMZ. We characterize PGW properties, seasonality, transport and mixing mechanisms to explain local processes influencing water mass transformation and oxygen fluxes into the OMZ. Atmospheric forcing at the source region and eddy mesoscale activity in the Gulf of Oman control spatiotemporal variability of PGW as it flows along-shelf off the northern Omani coast. Subseasonally, it is modulated by stirring and shear-driven mixing driven by eddy-topography interactions. The oxygen transport from PGW to the OMZ is estimated to be 1.3 Tmol yr^{-1} over the observational period, with dramatic inter- and intra-annual variability (± 1.6 Tmol yr^{-1}). We show that this oxygen is supplied to the interior of the OMZ through the combined action of double-diffusive and shear-driven mixing. Intermittent shear-driven mixing enhances double-diffusive processes, with mechanical shear conditions (Ri < 0.25) prevailing 14% of the time at the oxycline. These findings enhance our understanding of fine-scale processes influencing oxygen dynamics within the OMZ that can provide insights for improved modeling and prediction efforts.

Plain Language Summary The Arabian Sea hosts extremely low-oxygenated waters at depth (oxygen minimum zone, OMZ). Understanding how the depth of this layer changes and what processes control its variability is vital to understanding how it will change under climate change and how it may affect the ecosystem. One of the ways the oxygen gets into this low-oxygenated region is through the sinking of a water type called Persian Gulf Water (PGW). This water forms in the Persian Gulf and is hypersaline, warm, and well-oxygenated. It leaves the Persian Gulf through the narrow Strait of Hormuz and flows around 200 m depth along the northern coast of Oman. High-resolution ocean glider observations show the variability of its properties across different seasons and years. The amount of oxygen the PGW brings varies a lot over time, changing from year to year and between seasons. We estimate it to be 1.3 Tmol per year during the study period. We identify events, locations and mixing mechanisms that explain how the oxygen contained in PGW can mix with the surrounding low-oxygen waters, hence increasing the OMZ's oxygen content. This knowledge can be useful for improving climate models and predicting how the OMZ might change in the future.

1. Introduction

Persian Gulf Water (PGW) is distinguished by its high salinity (>40 g kg^{-1}) and high oxygen content (Brewer & Dyrssen, 1985; Swift and Bower, 2003). PGW forms at a low rate, with estimates ranging from 0.15 to 0.21 Sv through extremely high evaporation and restricted exchange with the open ocean in the Persian Gulf (Yao and Johns, 2010). PGW is released in short pulses as a dense bottom current through the narrow and shallow Strait of Hormuz (roughly 50 km wide and 90 m deep); it then cascades down the continental slope and entrains less dense water until it reaches neutral buoyancy at depths between 200 and 250 m. Under the influence of the Coriolis force, PGW follows the southern boundary of the Gulf of Oman as a gravity-adjusted flow (Bower et al., 2000) where eddy-outflow interactions are expected (Vic et al., 2015). Finally, it spreads laterally into the Arabian Sea and the Indian Ocean (Bower et al., 2000; Ezam et al., 2010; Prasad et al., 2001) and its high-salinity, high-oxygen

Supervision: Sebastiaan Swart, Bastien Y. Queste

Validation: Bastien Y. Queste

Visualization: Estel Font

Writing – original draft: Estel Font

Writing – review & editing: Estel Font, Sebastiaan Swart, Gerd Bruss, Peter M. F. Sheehan, Karen J. Heywood, Bastien Y. Queste

signature may be detected as far away as the Bay of Bengal (Jain et al., 2017; Sheehan et al., 2020) and the Agulhas Leakage (Durgadoo et al., 2017). Our understanding of the spatial and temporal variability of PGW and its interactions with surrounding water masses, particularly at depth and at small spatial scales remains constrained by low-resolution models and sparse observations in both space and time.

Within the Gulf of Oman, dynamical processes, such as mesoscale eddy field strain and eddy-topography interactions, are key to setting the open-ocean properties of PGW (Vic et al., 2015; L'Hégaret et al., 2015, 2016; Queste, Vic, et al., 2018). The interaction between mesoscale eddies and the steep slope of the continental shelf results in the generation of numerous smaller eddies, known as "peddies," via frictional boundary layers that arise from eddy-topography interactions (Queste, Vic, et al., 2018; Vic et al., 2015). Vic et al. (2015) suggest that the primary mechanism of peddy formation is the mesoscale field interacting with the slope, which generates vortices that trap PGW. These vortices then deform and break up under external shear and strain (L'Hégaret et al., 2016), recirculate within the Gulf of Oman and PGW is diluted. Furthermore, previous studies have described double-diffusive conditions (salt fingering; Turner, 1967) beneath PGW in the Arabian Sea (L'Hégaret et al., 2021). Salt fingering is a type of double diffusion that occurs when temperature and salinity gradients have the same sign: where warm and saline water (spicy) overlays colder and fresher water (minty). Moreover, evidence suggests that shear can enhance dissipation resulting from double diffusion and increase the potential for heat, salt, and other properties, such as oxygen, to diffuse and mix (e.g., the rate of dissipation of turbulent kinetic energy is 47% larger in observations where double diffusion coexists with shear instabilities, compared to where only double diffusive conditions are present; Fine et al., 2022). The volume and property transport toward the Arabian Sea, and the contribution of both lateral stirring and vertical mixing to the ventilation of intermediate water masses, remain poorly understood. Specifically, the influence of mesoscale eddies and buoyancy- and shear-driven mixing on the characteristics and circulation of PGW at seasonal and annual scales has not been quantified.

The oxygen minimum zone (OMZ) of the Arabian Sea is the most intense in the world, with suboxia (<6 μmol kg^{-1}) prevailing across most of the intermediate ocean (150–1,250 m) in its northern (e.g., Gulf of Oman) and northeastern parts (Rixen et al., 2020; Schmidt et al., 2021). OMZs exhibit highly atypical biogeochemical pathways, and their role in the global cycling of carbon and nitrogen is disproportionate to their size, affecting the ecosystem (e.g., habitat compression) but also contributing to climate via greenhouse outgassing (Gruber & Galloway, 2008; Hood et al., 2023; Stramma et al., 2010). The Arabian Sea OMZ is characterized by a tight balance between biological and physical oxygen supply and consumption mechanisms, modulated by the monsoon cycle (Acharya & Panigrahi, 2016; Rixen et al., 2020). Oxygen ventilation is the process by which oxygen-rich surface waters are transported to deeper layers of the ocean (Luyten et al., 1982). Water masses formed in nearby regions, such as PGW, oxygenate more than a third (35%) of the Arabian Sea OMZ (Davila et al., 2023). PGW flows out just above the oxycline and, despite its small contribution in terms of water volume, it is an efficient source of ventilation on short time scales (months to years; Lachkar et al., 2023). Therefore, the Arabian Sea OMZ is likely to respond rapidly to changes in PGW properties (Ditkovsky et al., 2023; Lachkar et al., 2019). As such, and notwithstanding PGW's low formation rate, the production, modification, and export of PGW influence the salinity budget, productivity, carbon drawdown, and nitrogen cycling of this globally important region of the Indian Ocean. Accurate quantification of the amount of oxygen advected by this water mass from its source to the Arabian Sea is essential for estimating the contribution of PGW to the oxygen supply within the OMZ.

Here, we illustrate the temporal and spatial variability in PGW properties, stability, and transport along its primary outflow pathway through the Gulf of Oman at two key locations from four glider deployments spanning 18 months over a 4-year period. We quantify PGW oxygen transport at different parts of the annual cycle and propose a mechanistic hypothesis that supports the idea of dense water overflows, such as PGW, as critical for oxygen supply to the upper boundary of OMZs.

2. Observations

Observations over 18 months from four ocean gliders sampling on-off shelf in the southern Gulf of Oman cover an entire seasonal cycle at two locations (Figure 1a). Three Seagliders continuously occupied an 80 km transect between 23.65°N, 58.65°E and 24.25°N, 59°E in 2015 and 2016. Later, a SeaExplorer occupied a 50 km transect between 24.05°N, 57.5°E, and 24.5°N, 57.8°E in 2021 and 2022 (Figure 1a). All gliders sampled temperature,
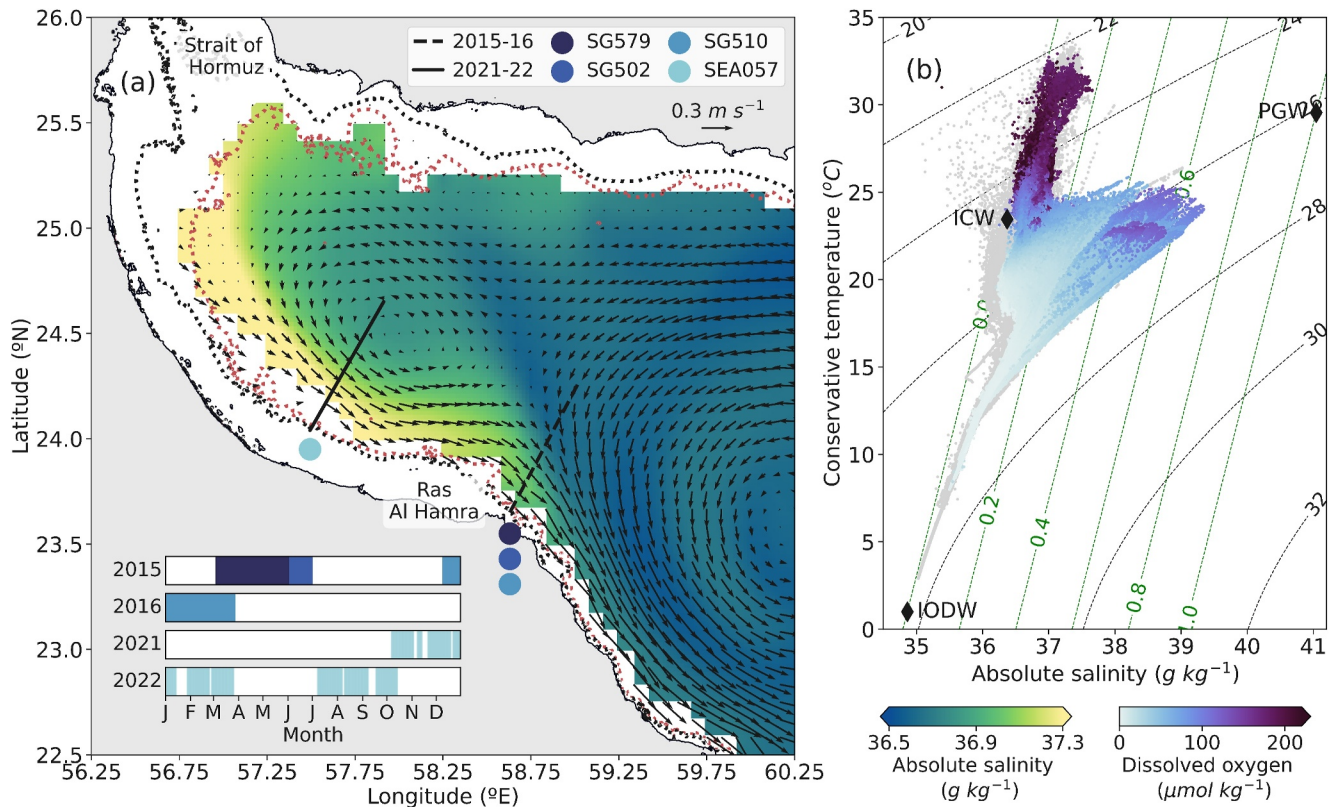
Figure 1. Glider campaigns in the Gulf of Oman. (a) Gulf of Oman map colored by a 20-year climatology of March absolute salinity at 200 m from GLORYS-12. Climatological surface geostrophic velocities from the same period and source are provided by the vectors. Contour lines show the coastline (black solid line), 100 m isobath (black dotted), and the shelf break at 300 m isobath (red dotted). The two black lines across the shelf denote the transect location during 2015–2016 (dashed) and 2021–2022 (solid), with the respective gliders that sampled those locations beneath the transect. Time series of the glider presence colored by the glider color-code. (b) T-S diagram of all glider data colored by dissolved oxygen concentration and climatology of ARGO data in the region determined by the map from 2012 to 2022 (gray). Contour lines show isopycnals (black) and PGW fraction isolines (green). Diamonds mark the three water mass endpoints used for the composite-tracer method.

salinity, and oxygen; in addition, SEA057 was equipped with an ADCP. For sensor and sampling specifications, see Table 1. Seaglider observations are processed following Queste, Vic, et al. (2018). SeaExplorer temperature and salinity observations are corrected following the manufacturer's instructions (M. Dever, pers. comm.). Ocean currents are computed using integration of vertical shear profiles from the ADCP and referenced to the glider's de-tided dive-average currents (Queste et al., 2023). The currents are rotated to along- and across-shelf co-ordinates (i.e., normal and parallel to the transect) using a clockwise rotation of 25°. Observations are projected onto a straight across-shelf line (Figure 1a) and median-binned onto a 2 m (vertical) by 1 km (horizontal, origin of coordinates: 300 m isobath) grid. Binned sections are interpolated vertically and horizontally to fill gaps, and

Table 1
Summary of the Glider Campaigns

Platform	Deployment	Recovery	Total days	Maximum depth range	Number of profiles	Number of transects	Sensors
SG579	04/03/2015	03/06/2015	90	100–1,000	1,424	25**	CTD[1] - O_2[3]
SG502	03/06/2015	30/06/2015	27	100–1,000	380	7	CTD[1] - O_2[3]
SG510	09/12/2015	26/03/2016	108	100–1,000	1,630	26	CTD[1] - O_2[3]
SEA057	06/10/2021	14/10/2022	223*	100–800	3,524	70***	CTD[2] - O_2[4] - ADCP[5]
TOTAL			368		6,958	128	

Note. The specifications and sampling frequency of the sensors are: (1) Seabird unpumped CTD - 0.2 Hz; (2) RBR Legato - 1 Hz; (3) Aanderaa 4330F DO - 0.2 Hz; (4) JFE Rinko - 1 Hz; and (5) Nortek 1,000 - 2m bins, 5s average, 3 beams. *Discontinuous, 9 missions (see Figure 1a). **No oxygen data during May 2015. *** 47 transects longer than 40 km. 10 transects were discarded due to biofouled sensor.

smoothed horizontally with a centered running mean of 3 km (Queste, Vic, et al., 2018). Prior to calculating geostrophic shear (SG579, SG502, and SG510), the projected, gridded sections were passed through a 31 km horizontal Tukey window filter with a cosine fraction of 0.5. Geostrophic velocity was then calculated by referencing the geostrophic shear to de-tided, section-orthogonal dive-average currents. Tidal velocities are obtained from the OSU TPXO Arabian Sea 1/60° configuration (Egbert & Erofeeva, 2002). The geostrophic velocity derivation resolves only the velocity component perpendicular to the section. From the ADCP observations, we determine that along-shelf velocities at the PGW depth (100–400 m) are 14 times larger on average than the across-shelf component, supporting the assumption that along-shelf velocities dominate and our geostrophic estimates resolve the majority of transport. Eddy kinetic energy (EKE) is derived from the 1-year anomalies of the depth average currents from the glider and from surface geostrophic velocities from AVISO. The mean section of a property is computed as the mean of all occupations at each gridpoint of the gridded sections. The standard deviation section is computed as the standard deviation of the occupations at each gridpoint of the gridded sections. Mixed layer depth is defined using a density threshold of 0.125 kg m^{-3} (Font et al., 2022), and winter mode water as mode water trapped between spring surface stratification and the 25.2 kg m^{-3} isopycnal. Seasons are defined based on the surface mixed layer depth cycle (Summer: Mar–Oct; Winter: Nov–Feb).

3. Methods

3.1. Persian Gulf Water Fraction

We use the composite-tracer method to estimate the fraction of PGW in our observations (Rixen and Ittekkot, 2005; Schmidt et al., 2021). The three main source water masses in the Gulf of Oman are Indian Ocean Deep Water (IODW), Indian Central Water (ICW), and Persian Gulf Water (PGW) (Hupe & Karstensen, 2000; Rhein et al., 1997; Sastry et al., 1986) and are defined by characteristic conservative temperature and absolute salinity values at the source water mass (Figure 1b). The endpoints used in this study are IODW: 34.86 g kg^{-1}, 1°C; PGW: 41.04 g kg^{-1}, 29.56°C (Schmidt et al., 2021 based on World Ocean Atlas (WOA13)), and ICW: 36.37 g kg^{-1}, 23.45°C. Our definition of the ICW endpoint lies on the IODW-ICW mixing line defined by Schmidt et al. (2021), but our choice is distinguished by higher temperature and salinity relative to the endpoint they define for encompassing the observed PGW variability. All data points sitting outside the triangle defined by the three endpoints (Figure 1a) are not used in variables derived from PGW fraction (e.g., surface data in PGW volume and oxygen transport). We use the same endpoints for all the observational periods, although we acknowledge that the PGW endpoint is likely to vary seasonally and interannually due to different atmospheric forcing at the source (Lorenz et al., 2020). We quantify this variability with a sensitivity analysis of the PGW endpoint (Figure S1 in Supporting Information S1). The Schmidt et al. (2021) endpoint is warm and salty relative to the variability of PGW endpoints presented elsewhere (Lorenz et al., 2020). When estimating PGW using the range described by Lorenz et al. (2020), we find that we may underestimate PGW fraction by 15%. We utilize the Schmidt et al. (2021) endpoint as it provides a conservative estimate of PGW fraction and agrees better with temperature and salinity observations collected by the glider.

3.2. Transport

The total volume transport along the shelf is computed across the full transect as $\int P \cdot V_{along} dA$, where $P = 1$ for total volume transport, and P is the dissolved oxygen concentration for oxygen transport. V_{along} is the along-shelf component of the velocity field observed by the ADCP onboard of the glider during 2021–2022; or the geostrophic velocities derived from the glider density sections during 2015–2016. dA is each cross-sectional area ($dl \cdot dz = 1,000$m·2m). To calculate PGW volume transport, we scale our estimates using PGW fraction (P = PGW fraction).

We estimate the oxygen transport by PGW scaling the PGW volume transport by the oxygen content of PGW source water and by density. As such, PGW oxygen transport is defined as $\int P \cdot V_{along} dA$, where $P = \rho \cdot [O_2]_{PGW:sol} \cdot PGW_{fraction}$, ρ is the density of the grid cell, and $[O_2]_{PGW:sol}$ is the oxygen solubility at the PGW endpoint. This estimation of oxygen transport by PGW is supported by the near 1:1 relation between observed dissolved oxygen concentration and oxygen solubility of the endpoint scaled with PGW fraction (Figure S2 in Supporting Information S1). Oxygen transport estimates rely on the assumption that PGW is the only source of oxygen as it mixes with oxygen-depleted waters. By calculating transport using PGW fraction and oxygen solubility, rather than observed oxygen concentration, we are specifically able to account for ventilation of the

OMZ; ventilation later respired after outflow from the Strait, but occurring upstream of the glider section. We can thereby estimate the total oxygen transport into the OMZ. Note that our PGW endpoint also presents the lowest oxygen solubility of the range of PGW properties described by Lorenz et al. (2020) (Figure S1 in Supporting Information S1); as a result, we might be underestimating oxygen transport by 20%. Thus, we provide a conservative estimate of oxygen supply from PGW.

3.3. Water Column Stability

The susceptibility of thermohaline stratification to double-diffusive instability can be measured by the Turner angle (Tu; Ruddick, 1983) given by $Tu = tan^{-1}\left(\frac{\alpha\frac{\partial\theta}{\partial z} - \beta\frac{\partial S}{\partial z}}{\alpha\frac{\partial\theta}{\partial z} + \beta\frac{\partial S}{\partial z}}\right)$, where θ is temperature, S is salinity and α and β are coefficients of thermal expansion and haline contraction, respectively. When $|Tu| < 45°$, both thermal and haline stratification are stable (double stability; DS). A $|Tu| > 90°$ suggests an unstable water column (unstable; US), where $N^2 < 0$ (N^2 is Brunt–Väisälä frequency, a measure of stratification). The water column will be susceptible to double-diffusive instability in the salt fingering regime when $45° < Tu < 90°$ (salt fingering; SF), and in the convective regime when $-90° < Tu < -45°$ (diffusive convection; DC). Double-diffusive instabilities can natural promote mixing due to different diffusion rates for heat and salt, while doubly stable environments will only mix from input of kinetic energy.

In addition, the gradient Richardson number is defined as $Ri = \frac{N^2}{S^2}$, where $S^2 = \frac{\partial u}{\partial z}^2 + \frac{\partial v}{\partial z}^2$ is the vertical shear and u and v are the zonal and meridional velocity components measured by the glider ADCP. Ri can be used to infer the prevalence of shear instabilities – an environment is prone to vigorous mixing, through input of kinetic energy as mentioned above, for Ri < 0.25, given that the vertical shear (S) is much greater than the stratification (N^2).

4. Results and Discussion

4.1. Mean State and Variability of PGW Outflow Properties

Hydrographic glider observations offshore of the northern coast of Oman reveal the temporal and spatial extent and variability in the properties of PGW (Figure 2 and Figure S3 in Supporting Information S1). PGW outflow is primarily concentrated along the continental slope within a potential density range from 25.5 to 27 kg m^{-3}, corresponding to depths from 150 to 400 m (Figures 2 and 3); its core is located at a depth of 200 m (Figure 3). During 2021–2022, PGW outflow absolute salinity ranges from 36 to 39 g kg^{-1}, its conservative temperatures from 15 to 25.5°C, and its oxygen concentrations from 50 to 150 µmol kg^{-1} (Figures 1b and 2). The warmest waters are observed during December 2021 (25.5°C) and the saltiest during August 2021 (39 g kg^{-1}; Figure 2). Higher PGW fraction is observed during summer, with an average value of 0.35 and maximum values reaching 0.65 (Figure 3c). These periods of increased PGW fraction are associated with higher oxygen levels (Figures 1b and 2). The lowest PGW fraction is observed during winter (PGW fraction ≤ 0.2; Figure 3c). Additionally, PGW density is on average 26.5 kg m^{-3} during the summer, contrasting with a bimodal density distribution during winter, with a PGW fraction peak at the same density as in summer and a lighter peak around 25.7 kg m^{-3} (Figure 3d). The lighter waters observed during winter can be attributed to PGW being less saline compared to summer, which change is only partially compensated for by temperature. During 2015–2016, density and salinity present similar ranges to 2021–2022, while on average (Figure S4 in Supporting Information S1), waters are 1.5°C cooler based on the month-to-month comparison between 2015–2016 and 2021–2022 (not shown). The maximum temperature and salinity observed during 2015–2016 are in June 2015 (23.5°C, 38.75 g kg^{-1}; Figure S3 in Supporting Information S1). The mean PGW fraction is 0.21, presenting higher values during summer compared to winter, with a maximum of 0.55 (Figure S4 in Supporting Information S1). There is no contrasting signature in density between seasons (Figure S4 in Supporting Information S1).

The PGW core, defined as PGW confined to the shelf edge, when present, flows southeastward toward the Arabian Sea at an average speed of 0.15 ± 0.12 m s^{-1} throughout the observation period (Figure 3b and Figure S4 in Supporting Information S1). Maximum velocities are not observed where we observe the maximum PGW fraction. The maximum PGW fraction is located immediately adjacent to the shelf while maximum velocities are found 5–10 km away from the 300 m isobath (Figure 3b). Velocities are generally greater close to the upper boundary of the PGW layer (Figure 3). The core never reverses fully. For instance, in February 2022 the glider samples a strong anticyclonic eddy that reverses the flow of the full water column toward the northwest, yet the core of PGW by the shelf does not reverse (Figures 5a and 8g). PGW core velocities are highest during summer
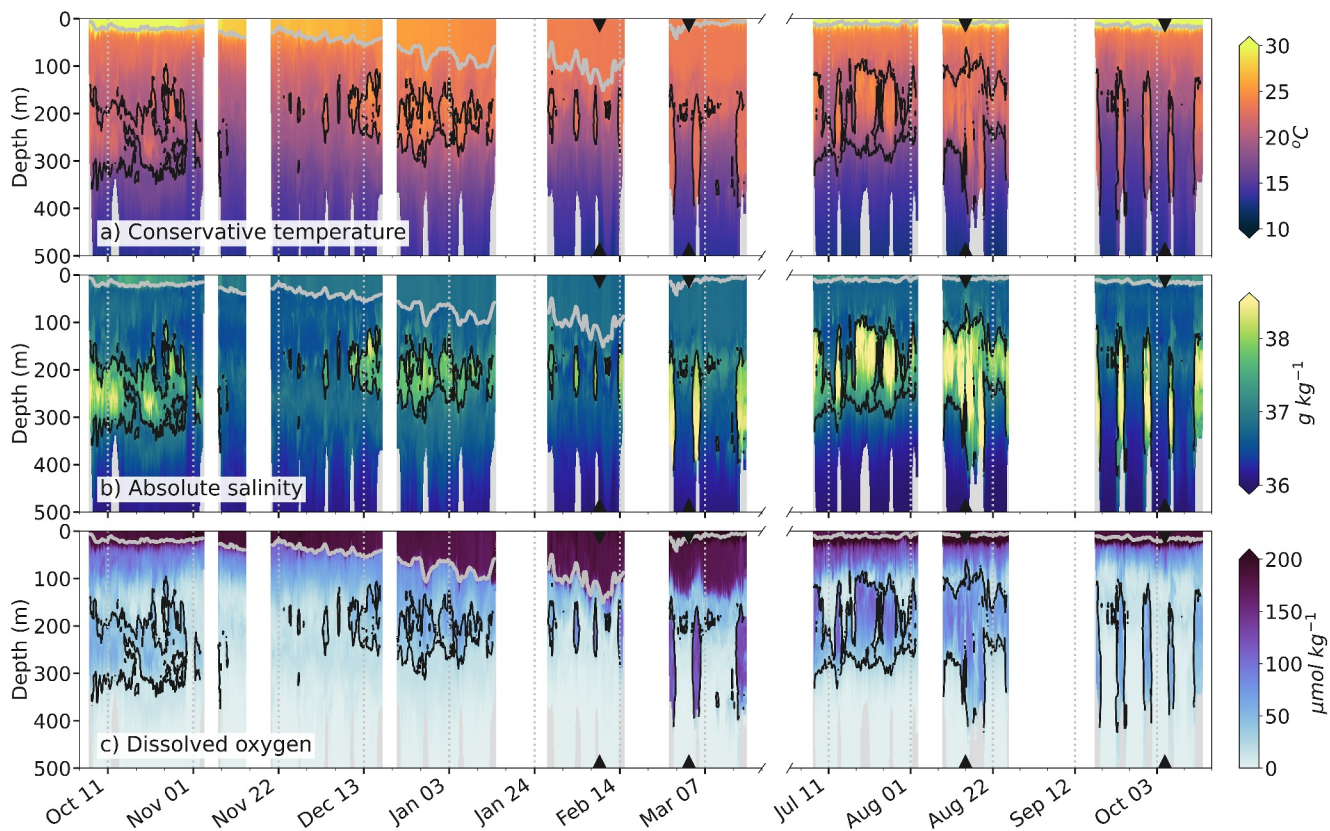
Figure 2. Time series of glider observations. (a) Conservative temperature, (b) absolute salinity, and (c) dissolved oxygen concentration time series as observed by gliders during 2021–2022. The 0.25 PGW fraction contour is shown in black and the mixed layer depth in gray. The bathymetry is colored in gray. The case study profiles in Figure 8 are marked using black triangles. The gray vertical lines indicate intervals of 21 days.

(Aug-Sep) peaking to 0.45 m s^{-1} southeastwards, when PGW outflow is concentrated by the shelf and experiences little shedding (Figure 5a).

Submesoscale PGW patches ("peddies"; Vic et al., 2015; L'Hégaret et al., 2016; Queste, Vic, et al., 2018) are observed offshelf (e.g., beginning of January or end of July in Figure 2). The standard deviation of PGW fraction reveals the occasional presence of this water mass away from the shelf (contours in Figures 3a and 3b). In periods with low mesoscale eddy activity (EKE < 0.01 m^2 s^{-2}; Figure 5b), PGW is concentrated near the shelf and no peddies are observed (e.g., Figures 2 and 5, Mar and Sep 2022). In contrast, a more energetic mesoscale field (EKE > 0.01 m^2 s^{-2}; Figure 5b) correlates with periods when there are more peddies off-shelf (e.g., Figures 2 and 5, Jan and Jul 2022). These observations support the mechanistic hypothesis of the mesoscale eddy field interacting with the shelf as driver of peddy formation stated by Vic et al. (2015) and observed by Queste, Vic, et al. (2018). These peddies that shed off-shelf have a high potential for oxygen ventilation, stirring the dissolved oxygen and leading to offshore transport of oxygen-rich water, and therefore influencing the depth of the oxycline. The mean flow in the Gulf of Oman determines whether these peddies are recirculated in the region, enhancing the dissipation of PGW locally, or whether they will be pushed toward the Arabian Sea.

The location of basin-scale eddies relative to the glider transect determines the large-scale flow observed by the gliders. In 2015–2016, the circulation of the Gulf of Oman is characterized by a typical mesoscale dipole (Pous, 2004; L'Hégaret et al., 2015), with an anticyclone located to the west and a cyclone to the east of Ras al Hamra (Figures 4a and 4b). From March to May 2015 the glider samples the region between the dipole (Figure 4a); there is little to no northwestward flow across the glider transect (not shown). Conversely, the flow is predominantly southeastward across the glider transect when the cyclonic mesoscale eddy occupies the center of the basin (Jun and Dec 2015 Jan 2016; Figure 4b). During 2021–2022, the mesoscale dipole is not present (Figure 4). From November to January, the surface currents are eastward, with a reversal at depth below the PGW layer (Figures 4c and 5a). In mid-January, the entire water column primarily flows westward (Figure 4d). In
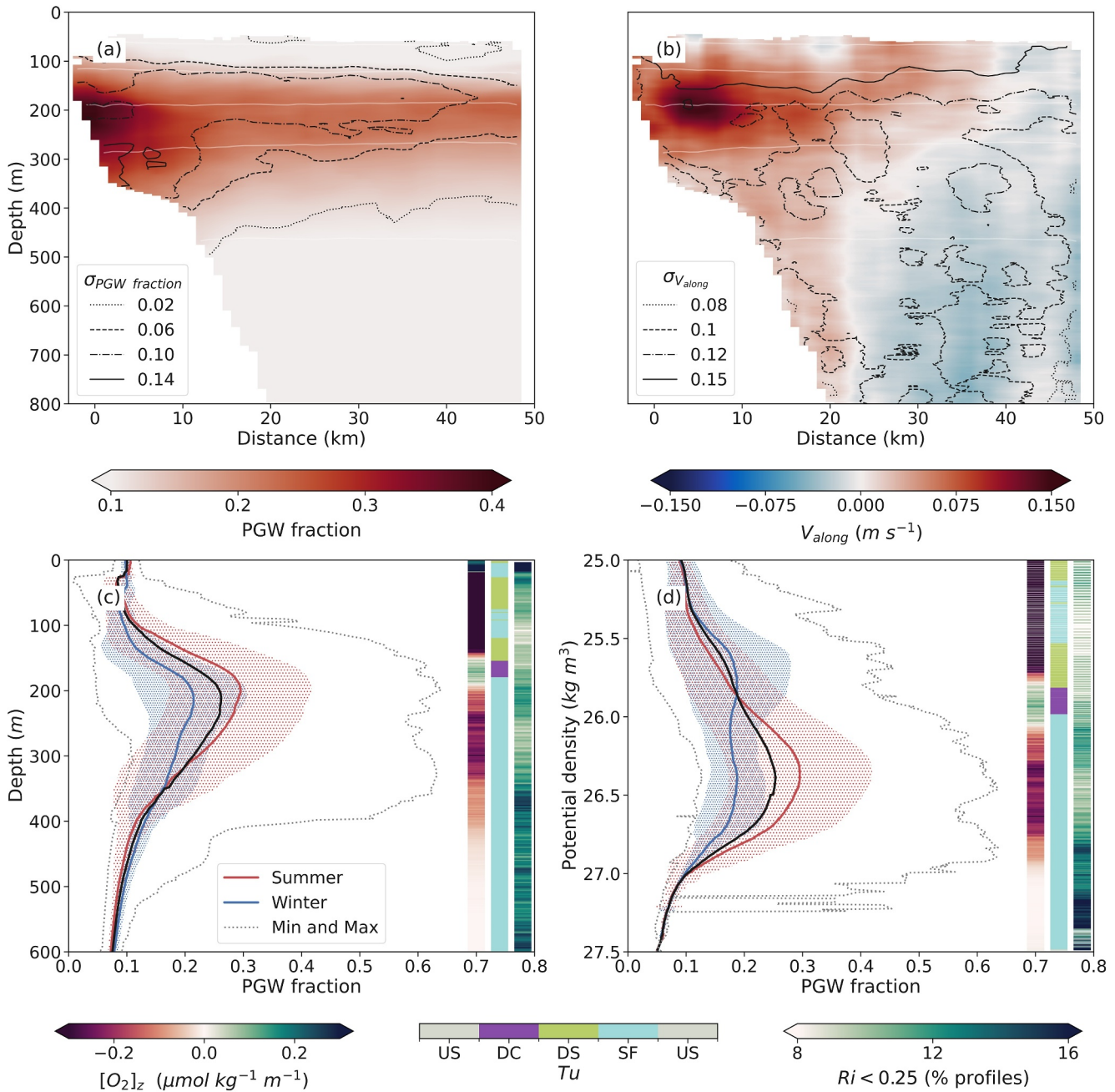
Figure 3. PGW spatiotemporal characteristics 2021–2022. (a) Mean PGW fraction and (b) mean along-shelf velocity section from the 2021-2022 campaign from transects longer than 40 km (48 of 70 transects). Contour lines show the respective standard deviations (σ) computed as described in Section 2. (c) Mean PGW fraction profiles with shaded standard deviation for summer and winter seasons in depth and (d) potential density space. The colored vertical bars along the right edge show the average vertical dissolved oxygen gradient ($[O_2]_z$), mode Turner angle (Tu, US, unstable; SF, salt fingering; DS, double stable; DC, diffusive convection), and percentage of profiles when the Ri < 0.25.

March, a smaller dipole forms on the western side of the basin, and the glider samples its anticyclone as the eddy moves closer to the coast (Figure 4e). By June, the anticyclone dissipates, and the cyclone becomes the dominant feature in the western basin, causing a shift in the flow toward the southeast for the remainder of the sampling period (Figure 4d). These differences in the mesoscale eddy field can result in different pathways of circulation of PGW, which result in different residence times in the Gulf of Oman that can lead to varying dilution rates and density classes of PGW through greater exposure to mixing. This could be the cause of the observed bimodal PGW density during winter 2021–2022 (Figure 2d). The lighter PGW could have had more exposure to mixing
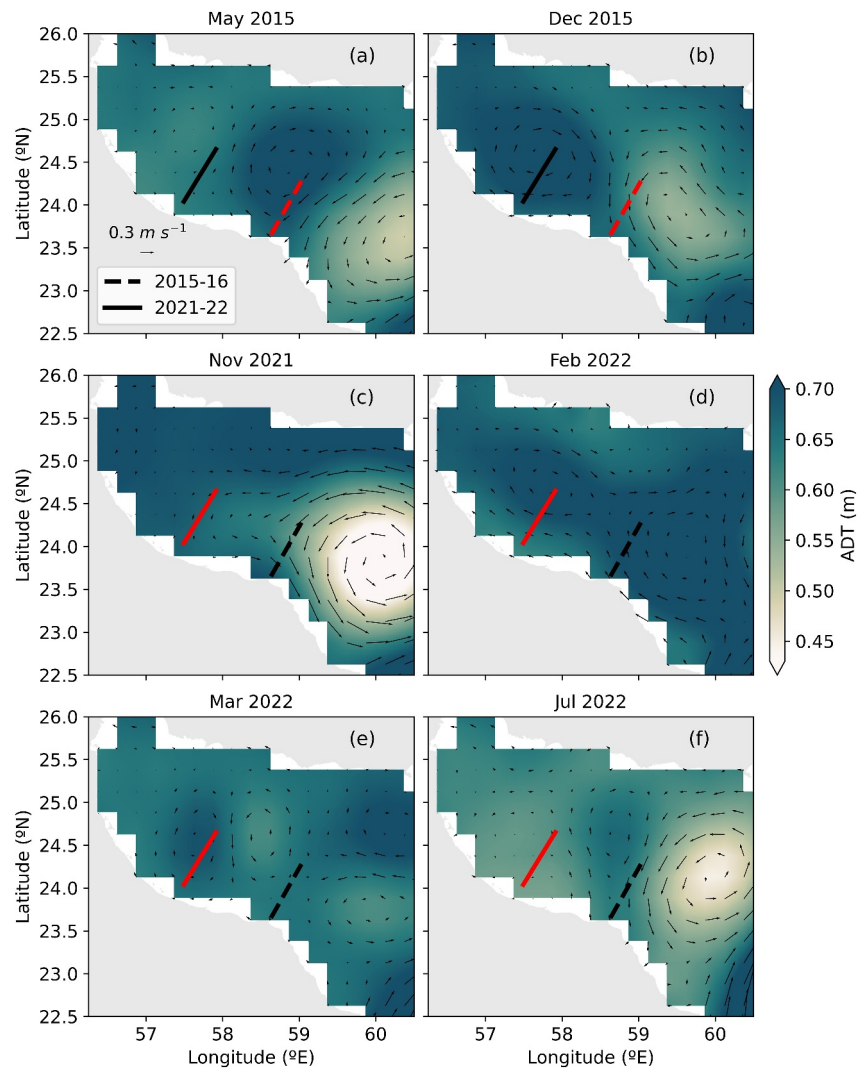
Figure 4. Mesoscale eddy field. Monthly mean of the absolute dynamic topography (ADT, colormap) and surface geostrophic velocities (arrows) from AVISO for selected months to illustrate the mesoscale variability in the Gulf of Oman. (a) April 2015, (b) December 2015, (c) November 2021, (d) February 2022, (e) March 2022 and (f) July 2022. The two lines across the shelf denote the transect location during 2015–2016 (dashed) and 2021–2022 (solid). The transect location of the glider deployment for the respective year is colored in red. We supplement this figure with an animation of daily ADT across the 4-year period in the Gulf of Oman (Figure S6 in Supporting Information S1).

than the denser peak due to different residence times on the western side of the Gulf of Oman. Moreover, previous studies indicate warmer, saltier and greater outflow during wintertime at the Strait of Hormuz (Bower et al., 2000; Johns et al., 2003; Pous, 2004). This differs with our observations, as we observe lower PGW fractions in winter. We hypothesize that winter-sampled PGW off the northern coast of Oman may be linked to PGW formed and exported out of the Persian Gulf in late summer, and recirculation might be crucial in setting the PGW properties that we observe, as previously suggested by Queste, Vic, et al. (2018); see their Figure 3.

4.2. Volume and Oxygen Transport

The net volume transport integrated across the transect observed by the gliders, calculated as the mean over 48 sections, is 0.5 ± 2.8 Sv. During summer, the volume transport is predominantly directed toward the Arabian Sea with an average over 34 occupations of 1.2 ± 2.7 Sv. In winter it tends to be toward the northwest (−0.5 ± 2.6 Sv, 14 occupations). Large standard deviations in transport highlight the high variability of the system in time (Figure 5d, mean transport per transect), but also in space (on-off shelf, e.g. Sep–Oct 2022 in Figures 5a and 5d
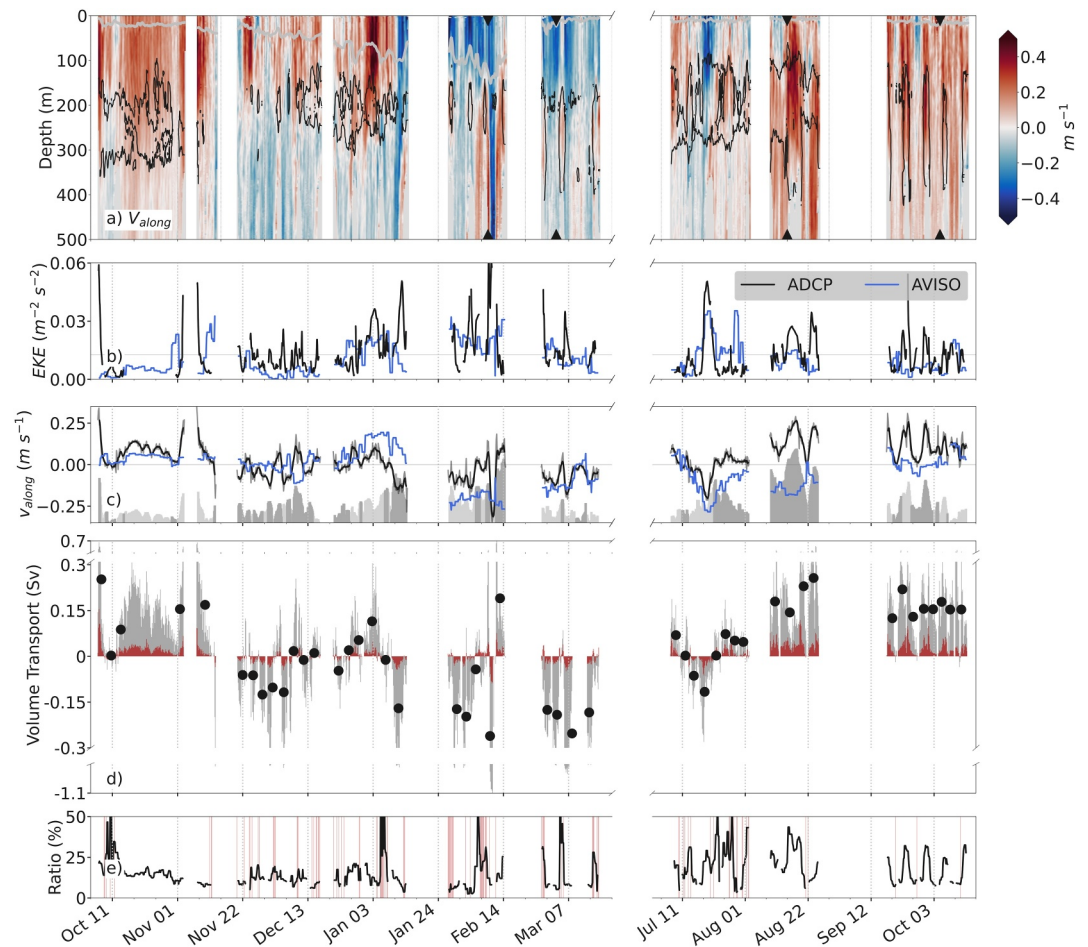
Figure 5. PGW volume transport. (a) Along-shelf velocity time series as observed by gliders during 2021–2022. The 0.25 PGW fraction contour is shown in black and the mixed layer depth in gray. The bathymetry is colored in gray. (b) Eddy kinetic energy (EKE) from the glider (black line) and from surface geostrophic velocities from AVISO. (c) Water column-averaged along-shelf velocity from the glider ADCP (black line) and absolute surface geostrophic velocities at the glider location (AVISO, blue line). Gray shading bars show the difference between the two velocity estimates and darker sharding when opposing directions. (d) Full-depth volume transport (gray) and PGW volume transport (red) per kilometer. The black dots show the mean total transport per transect. (e) The ratio of PGW volume transport to total volume transport. The red vertical lines show when PGW transport opposes net volume transport. The gray vertical lines indicate intervals of 15 days.

with increased eastward transport close to the shelf). Volume transport derived from the glider observations is controlled by the strength and the direction of the along–shelf component of the geostrophic velocity derived from AVISO (Figure 5b), but strongly modulated by the presence of PGW at depth (hours to days and on-offshore O(1–10 km); Figure 5d). Neither the PGW core nor peddies have a sea surface height signature (not shown), thus the magnitude and variability of the volume transport cannot be estimated and monitored using remote sensing techniques. We illustrate this fact by showing the difference in magnitude and direction between the along-shelf component of the surface geostrophic flow derived from sea surface height observations and the depth-averaged flow from the gliders (Figure 5c). Geostrophic velocities derived from altimetry cannot resolve the ageostrophic flows that might appear at depth such as mid-water eddies, or the PGW current by the shelf. Hence there is a need for full-depth transport observations that can resolve the ageostrophic features of the flow, such as the glider observations presented in this work, to represent PGW and oxygen transport accurately.

The volume transport of PGW is 0.16 ± 0.39 Sv on average, contributing 35% to the total transport (Figure 5). This estimate is in agreement with other literature estimates at the Strait of Hormuz (0.15–0.21 Sv annually; Johns et al., 2003; Pous, 2004; Yao and Johns, 2010). PGW generally flows in the same direction as the total transport, opposing it only 6% of the time (Figure 5e). For instance, when the general direction of advection shifts to the
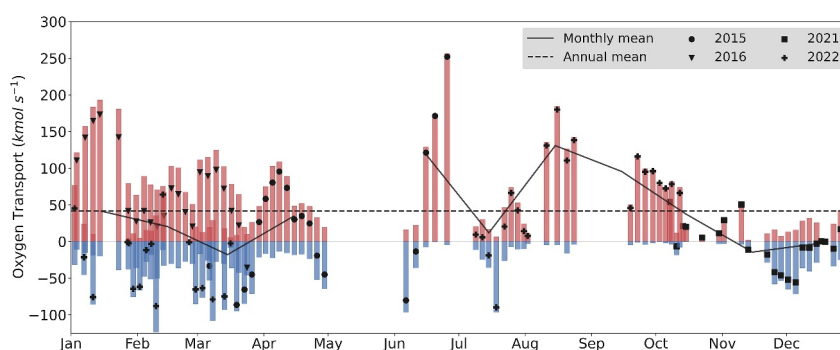
Figure 6. PGW oxygen transport. Annual cycle of PGW oxygen along-shelf transport across a 35 km transect from the 300 m isobath from the glider observations from direct measurements (2021–2022) and derived geostrophic velocities (2015–2016) (Net transport (black dots) = positive transport (red bars) + negative transport (blue bars)). Positive transport is directed along the shelf toward the Arabian Sea and negative transport along the shelf toward the Persian Gulf. Monthly averages are indicated using a solid line and the annual mean using a dashed line.

northwest, the PGW core still flows toward the Arabian Sea closer to the shelf (Jan–Mar 2022, Figure 5a). The patchiness generated by peddy occurrence across the glider sections does not always reduce PGW transport (e.g., August 2022 in Figure 3d). The PGW volume transport during summer is 0.30 ± 0.40 Sv and -0.02 ± 0.26 Sv during winter. Despite large standard deviation in the seasonal transport estimates, observations suggest seasonality with more stable unidirectional eastward flow from August to October and more variability during the rest of the year (Figure 5d). These results are in disagreement with previous studies that have described a relatively steady PGW outflow throughout the year, with little variation in seasonal timescales (Johns et al., 2003; Schmidt et al., 2020). The glider observations of the seasonality in PGW properties and transport should not be interpreted as the seasonality of the outflow at the Strait of Hormuz, given the recirculation and residence times in the Gulf of Oman (Queste, Vic, et al., 2018). We note that the outflow volume transport could present little seasonal variation at the Strait of Hormuz, and the variability we observe could be attributed to recirculation in the western side of the Gulf of Oman (Queste, Vic, et al., 2018).

The oxygen transport by PGW across the transect is determined by multiplying the PGW transport by the oxygen solubility of the PGW endpoint (Section 3.2, Figure S2 in Supporting Information S1). The time series of oxygen transport by PGW is extended using the 2015–2016 glider along-shelf geostrophic velocity sections to represent a full annual cycle (Section 3.2, Figure 6). Oxygen transport estimates indicate how much oxygen is brought by PGW into the OMZ, and should not be understood as simply responding to the seasonality of the outflow at the Strait of Hormuz. We determine that the annual cumulative oxygen transport across the transect is 1.3 Tmol yr^{-1} toward the Arabian Sea computed as the annual mean of the monthly average oxygen transport across the transect (to weigh each month equally) and then integrated over a year. This results in a net positive transport of oxygen toward the Arabian Sea. Our estimate is in agreement with modeling studies that determine that, despite PGW's relatively small contribution in terms of volume transport, it is an important driver of ventilation over time scales of months to years. Lachkar et al. (2023) found that PGW represents 2.5% of the total supply of oxygen to the OMZ, with this estimate increasing to 6.3% when considering only the upper OMZ.

PGW oxygen transport exhibits intra- and inter-annual variability in the direction of the flow and magnitude (Figure 6). The oxygen transport exhibits intra-annual variability across different months, similar to the variability of the total net volume and PGW transport previously described in Figure 5c. This results in an intra-annual standard deviation in oxygen transport of ± 1.6 Tmol yr^{-1} (-0.3 to 2.9 Tmol yr^{-1}). We assess the interannual variability of the oxygen transport during March, which was observed across three different years. The average oxygen transport during March is -0.04 ± 0.13 Tmol mth^{-1} (2015: -0.10 Tmol mth^{-1}; 2016: 0.14 Tmol mth^{-1}; and 2022: -0.14 Tmol mth^{-1}). We hypothesize that the large variability in oxygen transport during March across different years could be attributed to differences in the mesoscale activity of the different locations sampled (Section 4.1 and Figure 4), monsoon strength that influences the circulation in the Arabian Sea (Schmidt et al., 2020); and climate modes such as El Niño affecting 2015–2016 PGW endpoint.

The total oxygen transport estimation presents certain limitations. We present the only known time series of PGW oxygen transport resolving across shelf sections covering all seasons over more than a year. Despite the high resolution nature of the observations, it is not possible to infer a climatological transport estimate due to the evident intra- and inter-annual variability in transport. We acknowledge that we might underestimate the total transport to the Arabian Sea OMZ due to other circulation pathways of PGW from the strait (e.g., toward the coast of Iran); that some of this oxygen will mix locally in the Gulf of Oman (Queste, Vic, et al., 2018); or will be advected past the Arabian Sea toward the Bay of Bengal and/or southern Indian Ocean (Durgadoo et al., 2017; Jain et al., 2017; Sheehan et al., 2020). Furthermore, uncertainties in the estimate arise from our choice of a constant PGW end-point (and oxygen solubility) rather than resolving variability at the Strait of Hormuz. Despite these assumptions, our observations highlight the criticality of events at timescales shorter than monthly enhancing the oxygen transport toward the Arabian Sea and thus impacting the variability of the upper OMZ oxycline. With microbial carbon and nitrogen pathways varying greatly between anoxic, suboxic, and hypoxic regimes, it is likely that ventilation of the upper OMZ by PGW will have significant impacts on carbon remineralization rates, export efficiency, and nitrogen removal (Le Moigne et al., 2017).

4.3. PGW Instabilities and Ventilation Potential

Constraining how much of the PGW is mixed into the OMZ locally will provide a better understanding of how much PGW flows out beyond the Arabian Sea OMZ and the spatial variability of OMZ ventilation. A key driver of oxygen ventilation is double-diffusive instabilities. The glider observations reveal a double-diffusive regime enveloping PGW throughout the glider time series. Turner angle between $45° < Tu < 90°$ representing salt fingering (SF) are present below PGW and angles between $-90° < Tu < -45°$ representing diffusive convection (DC) are present above PGW (SF-blue and DC-purple in Figures 3c and 7 for the 2021–2022 campaign; and Figures S3–S5 in Supporting Information S1 for the 2015–2016 campaigns) in accordance with previous observational studies (e.g., L'Hégaret et al. (2021)). Moreover, double-diffusive conditions coexist in space and time with strong oxygen gradients (Figures 3c and 7) highlighting the potential of double-diffusive instabilities to drive diapycnal exchanges of oxygen.

Although we find a salt fingering regime in the Arabian Sea typically extending from the thermocline to the seafloor (You, 2002), inflow of PGW serves to not only increase the Turner angle (i.e., salt fingering conditions) but also increase the vertical oxygen gradient. Consequently, salt fingering processes have the potential to promote diapycnal mixing of oxygen below the PGW and therefore ventilate the OMZ. This is likely to be ubiquitous where PGW is present due to the warm, haline and oxygenated nature of PGW compared to the surrounding colder, fresher and less oxygenated water masses, and will contribute to gradual ventilation with little temporal variability.

Double diffusive conditions coexist with strong shear with the potential for mechanical mixing (Ri < 0.25, Figures 3 and 7). Potential for shear-driven mixing is present where boundary friction is expected (by the shelf, below the PGW core); at the base of mixed layers where surface velocities differ from deeper layers; during periods of large EKE (e.g., cyclonic eddy in Feb 2022, Figures 3b and 5b); and when and where peddies are present (i.e. between 200 and 300 m) (Figure 7c). To evaluate the temporal variability of shear effects, the fraction of time for each depth in which Ri < 0.25 is calculated (Figures 3c and 3d). Below the PGW fraction maxima, shear-driven instability conditions are observed in 14% of the profiles (Ri < 0.25 in Figure 3c), indicating the intermittent occurrence of potential for shear-driven mixing on a double-diffusive background regime (Figures 3 and 7). Previous studies suggest that double-diffusive background conditions can destabilize stratified shear flows leading to instabilities when and where Ri < 1 (Yang et al., 2023). If we consider Ri < 1, 37% of the profiles would indicate shear-driven mixing (not shown). Shear can enhance dissipation resulting from double diffusion and result in increased mixing of properties (Fine et al., 2022). The significance of instabilities driven by vertical shear in this region is that they could intermittently enhance mixing due to the interaction with double diffusion background conditions, and they occur where the strongest oxygen gradients are present (Figures 4 and 7a), leading to enhanced oxygen ventilation.

To elucidate the underlying mechanisms for oxygen ventilation present in the region, we select four exemplar sections that showcase different oxygen distribution. We present four case study transects: (1) a section with peddies (elevated PGW fraction spread along the transect, Figures 8a–8e); (2) a section where the PGW core is constrained to the shelf (Figures 8f–8j); (3) a strong cyclonic mesoscale eddy (Figures 8k–8o; elevated velocities
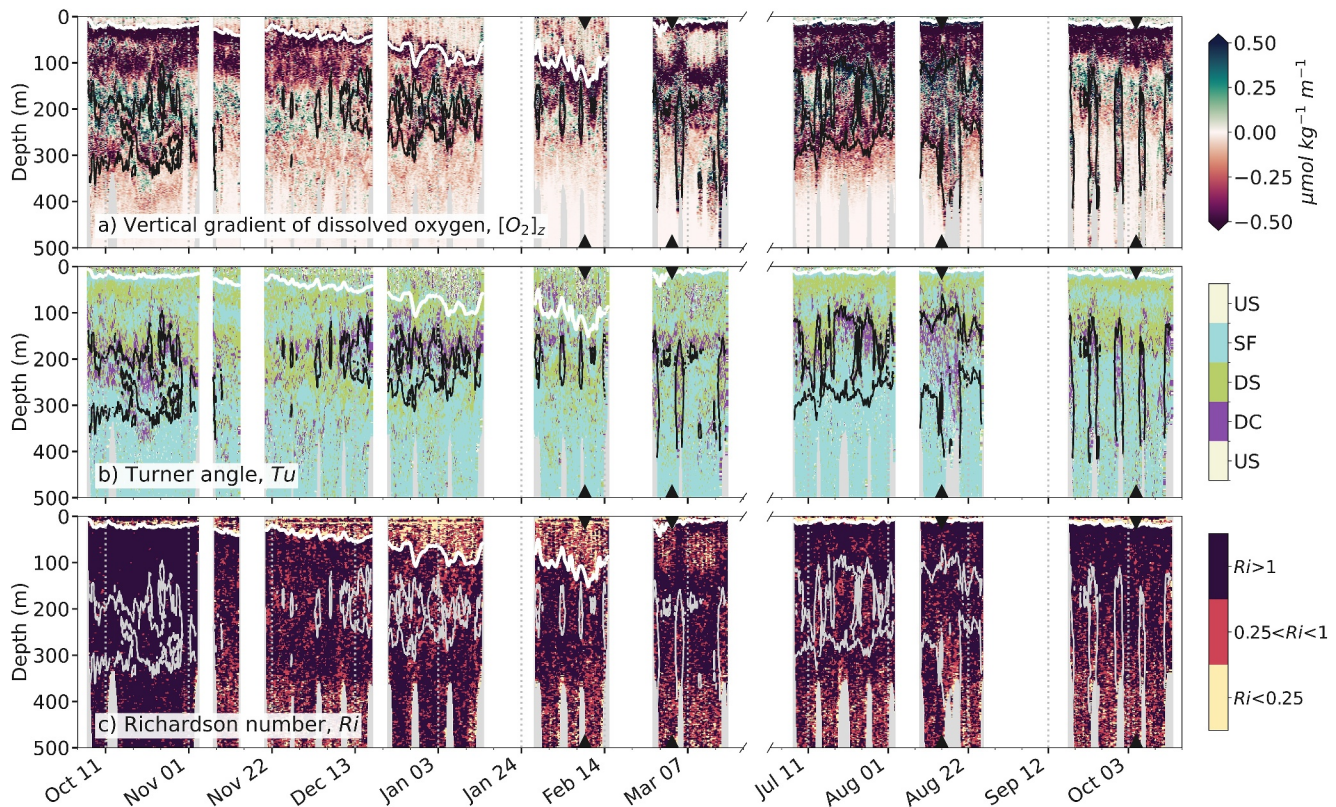
Figure 7. Water column instability. (a) Vertical gradient of dissolved oxygen ($[O_2]_z$), (b) Turner angle (Tu; US - unstable, SF - salt fingering, DS - double stable, and DC - diffusive convection), and (c) Richardson number (Ri) time series as observed by gliders during 2021–2022. The 0.25 PGW fraction contour is shown in black (a), (b) and gray (c); and the mixed layer depth in white. The bathymetry is colored in gray. The case study profiles in Figure 8 are marked using black triangles. The gray vertical lines indicate intervals of 21 days.

at depth and EKE $\gg 0.01 \, \text{m}^2 \, \text{s}^{-2}$, Figures 4d and 5b); and (4) an oxygenated deep coherent eddy (radius of 15 km at 400 m; Figures 8p–8t). The observed time series can be broken down into a combination of sections similar to case studies 1 and 2. The occurrence of these two regimes is 40% for spread PGW and 60% for a tight PGW core (Figure S5 in Supporting Information S1). The exemplar sections 3 and 4 are other examples of the regime illustrated in the case study 2, but with two eddy events that are present during 7 days each (two consecutive sections) and modify the oxygen distribution across the transect. These two examples highlight that intense mesoscale activity does not necessarily lead to spreading of PGW.

In all cases, PGW exhibits a pronounced high oxygen signature (first column in Figure 8), bounded by strong oxygen gradients, and characterized by double-diffusive regimes both above and below (third column in Figure 8). The largest potential for oxygen ventilation is where shear mixing (Ri < 0.25) coexists with strong vertical oxygen gradients ($[O_2]_z$). Therefore, we define a potential for oxygen ventilation index due to shear mixing potential ($[O_2]_z \cdot \text{Ri}^{-1}$, fourth column in Figure 8). Oxygen ventilation potential is enhanced below the core of the PGW close to the shelf, where the bottom boundary layer shear is elevated (observed in all four case studies). Oxygen ventilation potential is also enhanced below the mixed layer (Figure 8n), below the winter mode water layer (Figure 8i), and below the peddies that are stirred from the shelf toward the interior of the basin (Figure 8d). The hydrographic profiles for the peddies case study present a multilayered structure of different PGW fractions (Figure 8e), resulting from different mixing histories along its pathway from its origin (recirculation and dilution). Notably, staircasing is present when there is low shear (inside the coherent deep eddy in Figure 8t), but conspicuously absent where there is high shear (Figures 8e, 8j and 8o). Finally, the oxygenated deep coherent eddy (400 m, Figures 8p and 8q) is a clear example of the "cannonball eddy" concept described previously by Frenger et al. (2018). These submesoscale coherent vortices have been well-documented for several decades (McWilliams, 1985). Their physical and biogeochemical properties, such as salinity and oxygen, suggest that they originate from water masses located far from their observed positions, capturing and transporting waters
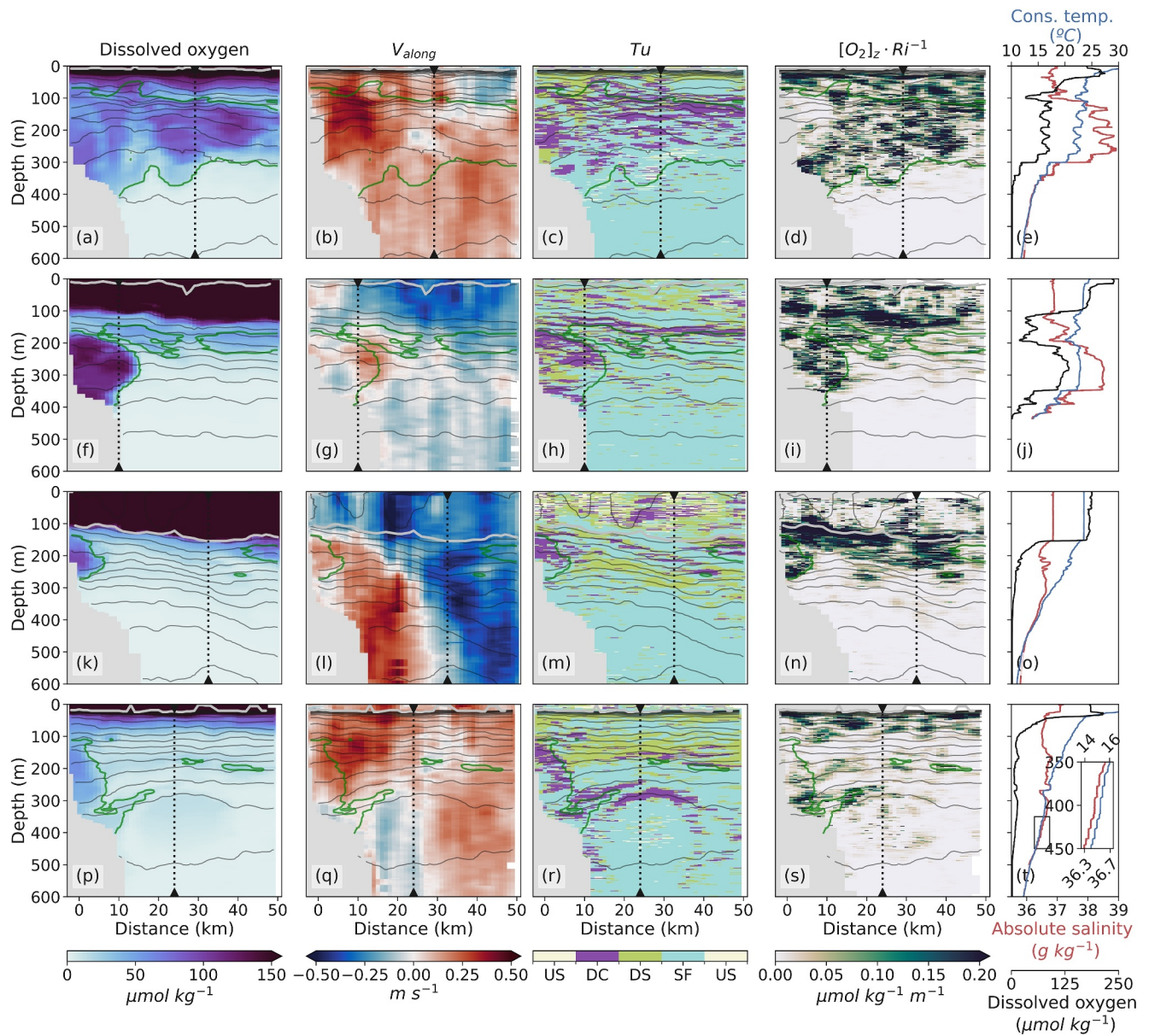
Figure 8. Case studies. Four exemplar sections (rows) based on distinct oxygen distributions across the section: (a)–(e) peddies, (f)–(j) intense PGW core, (k)–(o) mesoscale eddy (Figure 4d), and (p)–(t) oxygenated deep coherent eddy. The transect numbers are 56 (15 Aug 2022), 39 (03 Mar 2022), 32 (09 Feb 2022), and 70 (12 Oct 2022) respectively. These four case studies are marked in Figures 2, 5a and 7 (black triangles). Oxygen concentration (first column), along-shelf velocities (second column), Tu (third column), and potential for oxygen ventilation index $[O_2]_z \cdot Ri^{-1}$ (fourth column). The last column presents the profiles of conservative temperature, absolute salinity and dissolved oxygen referring to the vertical dotted black lines in the other panels (profile numbers 2,588, 1,734, 1,418, and 3,444). Isopycnals (black), 0.2 PGW fraction isoline (green), and mixed layer depth (gray) are shown in all panel sections. The bathymetry is colored in gray.

over extensive distances (O(100 km); for example, Frenger et al., 2018). These case studies highlight the large variability in the mechanisms that contribute to the colocation of strong shear mixing with strong vertical oxygen gradients on a double-diffusive background.

These novel observations of water column stability, shear, and oxygen capture the various mixing processes in the presence of strong oxygen gradients. Our results indicate that estimates of oxygen ventilation via salt fingering are a significant underestimation, as shown by the new body of literature that supports the hypotheses of dissipation enhancement through the interaction of mechanical mixing and double diffusion (e.g., Fine et al., 2022). Similar principles likely apply to other oxygenated dense water overflows such as Red Sea Water, and subducted surface

currents like the Southwest Monsoon Current toward the Bay of Bengal. Therefore, there is a need for quantifying how the coexistence of mechanical mixing and double diffusion enhances the magnitude of dissipation in the region to better estimate oxygen ventilation to the OMZ via these oxygenated subducted water masses.

Diapycnal transport of dissolved oxygen accomplished by mixing depends not only on the magnitude of that mixing but also on the magnitude of the vertical oxygen gradients. For example, the poor representation of dense outflows in numerical models leads to a misrepresentation of both mixing and vertical oxygen gradients. A key unknown today is how biological processes affect the vertical oxygen gradient in OMZ; variability in productivity, community composition and particulate export govern the sinking speed and remineralization rates which set biological oxygen demand vertically within the OMZ (Le Moigne et al., 2017). These processes merit significant attention, particularly considering that global climate models fail to reproduce observed deoxygenation changes (Ditkovsky et al., 2023; Oschlies et al., 2017; Schmidt et al., 2021). This failure is partly attributed to models' limited ability to resolve features smaller than their computational grid cells, such as overflow currents (Schmidt et al., 2021). Ditkovsky et al. (2023) suggest that alterations in advective ventilation pathways, such as PGW, play a crucial role in dissolved oxygen changes, and account for most simulated oxygen changes in the northern Arabian Sea. The buoyancy, oxygen content, and formation rate of PGW are sensitive to climate change: warming results in a reduction of oxygen solubility and thus a decline in oxygen levels in the Persian Gulf; heating and evaporation (warmer and saltier waters) increase the buoyancy of PGW at its source, weakening subduction to intermediate depths and reducing PGW contribution as an oxygen source to the Arabian Sea OMZ (Lachkar et al., 2019). Moreover, previous studies present the challenge of distinguishing projected changes in oxygen due to: mixing with surface waters; or changes in the source water types (Ditkovsky et al., 2023). We provide and describe a long time series of PGW buoyancy and advection observations that can support future studies to disentangle the effects of marginal sea shoaling and increase stratification in the projections of deoxygenation of the upper northern Arabian Sea OMZ. It must further be noted that earth system models discussed here model simplified biogeochemical cycling by necessity which may not represent community changes or response to fine scale processes accurately (Ditkovsky et al., 2023; Oschlies et al., 2017; Schmidt et al., 2021); particularly considering the impact of small scale processes on export efficiency (Guo et al., 2024). Furthermore, export efficiency and remineralization rates can vary greatly the range of oxygen concentrations considered hypoxic, further emphasizing the importance of resolving localized ventilation (Le Moigne et al., 2017; Queste, Vic, et al., 2018). Characterization of the intermediate circulation in the Arabian Sea, including dense outflows such as PGW, is needed to understand the associated variability of the OMZ, have accurate representation of source water types, have realistic oxygen projections under different climate scenarios, and related climate-biogeochemical interactions in global earth system models.

5. Conclusions

High-resolution glider observations spanning all seasons off the northern coast of Oman show sub-seasonal, seasonal, and interannual variability of PGW properties and transport and its key role in controlling the variability of the upper regional OMZ oxycline. We describe the temporal and spatial variability of PGW properties, presence, volume transport (total: 0.5 ± 2.8 Sv; PGW: 0.16 ± 0.39 Sv), and oxygen transport (1.3 Tmol yr^{-1}) along the northern coast of Oman toward the Arabian Sea. We observe high interannual (average across 3 different years of oxygen transport March: -0.04 ± 0.13 Tmol mth^{-1}) and intraseasonal (standard deviation of the monthly means of oxygen transport: ± 1.6 Tmol yr^{-1}) variability of oxygen transport. This variability is driven by the different locations of our glider sampling and thus different mesoscale activity and PGW circulation pathways. Our findings highlight the importance of high EKE periods on stirring PGW from the shelf toward the interior of the basin: there is a noticeable reduction in the presence of peddies during periods of low EKE. Current remote sensing methods are unable to fully describe the volume transport of PGW accurately. Hence, there is a need for full water column observations of transport.

The simultaneous observations of oxygen, water column stability, and shear allow us to resolve for the first time the mechanisms that can generate diapycnal turbulent mixing and oxygen ventilation. Shear is enhanced close to the shelf (bottom boundary layer), below the mixed layer and the winter mode water layer, and below the peddies. We determine that intermittent strong vertical shear is present below the PGW 14% of the time, where the largest oxygen gradients are located, coexisting with salt-fingering background conditions. The interaction between salt fingering and mechanical mixing can lead to enhanced oxygen ventilation toward the upper Arabian Sea OMZ. There is a need to quantify the rate and variability of oxygen diffusion toward the OMZ and quantify how the

coexistence of mechanical mixing and double diffusion enhances the magnitude of dissipation in the region. To address this aspect, direct measurements of mixing across the shelf and across different seasons along the PGW boundary are required.

Data Availability Statement

Seaglider data are available on request from the UEA Seaglider Facility and from the British Oceanographic Data Centre (Queste, Heywood, et al., 2018). SeaExplorer glider and ADCP data are available from Zenodo (Font & Queste, 2023). The GLORYS12V1 dataset (CMEMS, 2023b) is available from Copernicus Marine Environment Monitoring Service at https://doi.org/10.48670/moi-00021. The altimetry dataset (CMEMS, 2023a) is available from Copernicus Marine Environment Monitoring Service at https://doi.org/10.48670/moi-00149. The Argo data used in this study is available by the International Argo Program and the national programs that contribute to it. (time: 2000–2022; space: 56.2–61.5°E, 22–26°N; Argo, 2023). Bathymetry data is available by GEBCO Compilation Group (GEBCO, 2023). SeaExplorer data has been processed using https://github.com/bastienqueste/SeaExplorerTools (Queste, 2022), and the ADCP data as https://github.com/bastienqueste/glider-ad2cp (Queste et al., 2023). The software associated with this manuscript is published on GitHub https://github.com/EstelFont/PGW_transport_and_ventilation (Font, 2023).

References

Acharya, S. S., & Panigrahi, M. K. (2016). Eastward shift and maintenance of Arabian Sea oxygen minimum zone: Understanding the paradox. *Deep-Sea Research Part I Oceanographic Research Papers*, *115*, 240–252. https://doi.org/10.1016/j.dsr.2016.07.004

Argo. (2023). Argo float data and metadata from Global Data Assembly Centre (Argo GDAC). [Dataset]. *SEANOE*. https://doi.org/10.17882/42182

Bower, A. S., Hunt, H. D., & Price, J. F. (2000). Character and dynamics of the Red Sea and Persian Gulf outflows. *Journal of Geophysical Research: Oceans*, *105*(C3), 6387–6414. https://doi.org/10.1029/1999jc900297

Brewer, P. G., & Dyrssen, D. (1985). *Chemical Oceanography of the Persian Gulf* (Vol. 14, pp. 41–55).

CMEMS. (2023a). Global Ocean Gridded L4 Sea Surface Heights And Derived Variables Nrt. [Dataset]. *SEA-LEVEL_GLO_PHY_L4_NRT_OBSERVATIONS_008_046. E.U. Copernicus Marine Service Information (CMEMS). Marine Data Store (MDS)*. https://doi.org/10.48670/moi-00149

CMEMS. (2023b). Global ocean physics reanalysis. [Dataset]. *GLOBAL_MULTIYEAR_PHY_001_030. E.U. Copernicus Marine Service Information (CMEMS). Marine Data Store (MDS)*. https://doi.org/10.48670/moi-00021

Davila, X., Olsen, A., Lauvset, S. K., McDonagh, E. L., Brakstad, A., & Gebbie, G. (2023). On the origins of open ocean oxygen minimum zones. *Journal of Geophysical Research: Oceans*, *128*(8), e2023JC019677. https://doi.org/10.1029/2023JC019677

Ditkovsky, S., Resplandy, L., & Busecke, J. (2023). Unique ocean circulation pathways reshape the Indian Ocean oxygen minimum zone with warming. *Biogeosciences*, *20*(23), 4711–4736. https://doi.org/10.5194/bg-20-4711-2023

Durgadoo, J. V., Rühs, S., Biastoch, A., & Böning, C. W. B. (2017). Indian Ocean sources of Agulhas leakage. *Journal of Geophysical Research: Oceans*, *122*(4), 3481–3499. https://doi.org/10.1002/2016JC012676

Egbert, G. D., & Erofeeva, S. Y. (2002). Efficient inverse Modeling of Barotropic Ocean Tides. *Journal of Atmospheric and Oceanic Technology*, *19*(2), 183–204. https://doi.org/10.1175/1520-0426(2002)019<0183:EIMOBO>2.0.CO;2

Ezam, M., Bidokhti, A. A., & Javid, A. H. (2010). Numerical simulations of spreading of the Persian Gulf outflow into the Oman Sea. *Ocean Science*, *6*(4), 887–900. https://doi.org/10.5194/os-6-887-2010

Fine, E. C., Mackinnon, J. A., Alford, M. H., Middleton, L., Taylor, J., Mickett, J. B., et al. (2022). Double diffusion, shear instabilities, and heat impacts of a Pacific summer water intrusion in the Beaufort Sea. *Journal of Physical Oceanography*, *52*(2), 189–203. https://doi.org/10.1175/JPO-D-21-0074.1

Font, E. (2023). PGW transport and ventilation. [Software]. Retrieved from https://github.com/EstelFont/PGW_transport_and_ventilation

Font, E., & Queste, B. (2023). Processed glider data: 9 months of hydrographic and ADCP observations in the Gulf of Oman. (v1.0). [Dataset]. *Zenodo*. https://doi.org/10.5281/zenodo.10075774

Font, E., Queste, B. Y., & Swart, S. (2022). Seasonal to intraseasonal variability of the upper ocean mixed layer in the Gulf of Oman. *Journal of Geophysical Research: Oceans*, *127*(3). https://doi.org/10.1029/2021JC018045

Frenger, I., Bianchi, D., Stührenberg, C., Oschlies, A., Dunne, J., Deutsch, C., et al. (2018). Biogeochemical role of subsurface coherent eddies in the ocean: Tracer cannonballs, hypoxic storms, and microbial stewpots? *Global Biogeochemical Cycles*, *32*(2), 226–249. https://doi.org/10.1002/2017GB005743

GEBCO Compilation Group. (2023). GEBCO 2023 Grid. [Dataset]. https://doi.org/10.5285/f98b053b-0cbc-6c23-e053-6c86abc0af7b

Gruber, N., & Galloway, J. N. (2008). An Earth-system perspective of the global nitrogen cycle. *Nature*, *451*(7176), 293–296. https://doi.org/10.1038/nature06592

Guo, M., Xing, X., Xiu, P., Dall'Olmo, G., Chen, W., & Chai, F. (2024). Efficient biological carbon export to the mesopelagic ocean induced by submesoscale fronts. *Nature Communications*, *15*(1), 580. https://doi.org/10.1038/s41467-024-44846-7

Hood, R. R., Rixen, T., Lévy, M., Hansell, D. A., Coles, V. J., & Lachkar, Z. (2023). *Oxygen, carbon and pH variability in the Indian ocean*. In *Oceanography of the Indian Ocean*. Elsevier.

Hupe, A., & Karstensen, J. (2000). Redfield stoichiometry in Arabian Sea subsurface waters. *Global Biogeochemical Cycles*, *14*(1), 357–372. https://doi.org/10.1029/1999gb900077

Jain, V., Shankar, D., Vinayachandran, P. N., Kankonkar, A., Chatterjee, A., Amol, P., et al. (2017). Evidence for the existence of Persian Gulf Water and Red Sea Water in the Bay of Bengal. *Climate Dynamics*, *48*(9–10), 3207–3226. https://doi.org/10.1007/s00382-016-3259-4

Johns, W. E., Yao, F., Olson, D. B., Josey, S. A., Grist, J. P., & Smeed, D. A. (2003). Observations of seasonal exchange through the Straits of Hormuz and the inferred heat and freshwater budgets of the Persian Gulf. *Journal of Geophysical Research: Oceans*, *108*(12). https://doi.org/10.1029/2003jc001881

Lachkar, Z., Lévy, M., Hailegeorgis, D., & Vallivattathillam, P. (2023). Differences in recent and future trends in the Arabian Sea oxygen minimum zone: Processes and uncertainties. *Frontiers in Marine Science*, *10*. https://doi.org/10.3389/fmars.2023.1122043

Lachkar, Z., Lévy, M., & Smith, K. S. (2019). Strong intensification of the Arabian Sea Oxygen minimum zone in response to Arabian Gulf warming. *Geophysical Research Letters*, *46*(10), 5420–5429. https://doi.org/10.1029/2018GL081631

Le Moigne, F. A. C., Cisternas-Novoa, C., Piontek, J., Maßmig, M., & Engel, A. (2017). On the effect of low oxygen concentrations on bacterial degradation of sinking particles. *Scientific Reports*, *7*(1), 16722. https://doi.org/10.1038/s41598-017-16903-3

L'Hégaret, P., Carton, X., Louazel, S., & Boutin, G. (2016). Mesoscale eddies and submesoscale structures of Persian Gulf Water off the Omani coast in spring 2011. *Ocean Science*, *12*(3), 687–701. https://doi.org/10.5194/os-12-687-2016

L'Hégaret, P., Duarte, R., Carton, X., Vic, C., Ciani, D., Baraille, R., & Corréard, S. (2015). Mesoscale variability in the Arabian Sea from HYCOM model results and observations: Impact on the Persian Gulf Water path. *Ocean Science*, *11*(5), 667–693. https://doi.org/10.5194/os-11-667-2015

L'Hégaret, P., de Marez, C., Morvan, M., Meunier, T., & Carton, X. (2021). Spreading and vertical structure of the Persian Gulf and Red Sea outflows in the Northwestern Indian Ocean. *Journal of Geophysical Research: Oceans*, *126*(4). https://doi.org/10.1029/2019JC015983

Lorenz, M., Klingbeil, K., & Burchard, H. (2020). Numerical study of the exchange flow of the Persian Gulf using an extended total exchange flow analysis framework. *Journal of Geophysical Research: Oceans*, *125*(2), e2019JC015527. https://doi.org/10.1029/2019JC015527

Luyten, J. R., Pedlosky, J., & Stommel, H. (1982). The ventilated thermocline. *Journal of Physical Oceanography*, *13*(2), 292–309. https://doi.org/10.1175/1520-0485(1983)013<0292:tvt>2.0.co;2

McWilliams, J. C. (1985). Submesoscale, coherent vortices in the Ocean. *Reviews of Geophysics*, *23*(2), 165–182. https://doi.org/10.1029/rg023i002p00165

Oschlies, A., Duteil, O., Getzlaff, J., Koeve, W., Landolfi, A., & Schmidtko, S. (2017). Patterns of deoxygenation: Sensitivity to natural and anthropogenic drivers. *Philosophical Transactions of the Royal Society A: Mathematical, Physical & Engineering Sciences*, *375*(2102), 20160325. https://doi.org/10.1098/rsta.2016.0325

Pous, S. P., Carton, X., & Lazure, P. (2004). Hydrology and circulation in the Strait of Hormuz and the Gulf of Oman—Results from the GOGP99 Experiment: 2. Gulf of Oman. *Journal of Geophysical Research*, *109*(C12). https://doi.org/10.1029/2003jc002146

Prasad, T. G., Ikeda, M., & Kumar, S. P. (2001). Seasonal spreading of the Persian Gulf Water mass in the Arabian Sea. *Journal of Geophysical Research: Oceans*, *106*(C8), 17059–17071. https://doi.org/10.1029/2000jc000480

Queste, B. Y. (2022). SeaExplorer tools. [Software]. Retrieved from https://github.com/bastienqueste/SeaExplorerTools

Queste, B. Y., Heywood, K. J., & Piontkovski, S. A. (2018). Exploring the potential of ocean gliders: A pirate-proof technique to illuminate mesoscale physical-biological interactions off the coast of Oman (2015-2016). [Dataset]. *British Oceanographic Data Centre - Natural Environment Research Council, UK* https://doi.org/10.5285/697eb954-f60c-603b-e053-6c86abc00062

Queste, B. Y., Rollo, C., & Font, E. (2023). Glider AD2CP. [Software]. Retrieved from https://github.com/bastienqueste/gliderad2cp

Queste, B. Y., Vic, C., Heywood, K. J., & Piontkovski, S. A. (2018). Physical controls on oxygen distribution and denitrification potential in the North West Arabian Sea. *Geophysical Research Letters*, *45*(9), 4143–4152. https://doi.org/10.1029/2017GL076666

Rhein, M., Stramma, L., & Plähn, O. (1997). Tracer signals of the intermediate layer of the Arabian Sea. *Geophysical Research Letters*, *24*(21), 2561–2564. https://doi.org/10.1029/97GL01041

Rixen, T., Cowie, G., Gaye, B., Goes, J., Gomes, H. R., Hood, R., et al. (2020). Present past and future of the OMZ in the northern Indian Ocean. *Biogeosciences Discussions*. https://doi.org/10.5194/bg-2020-82

Rixen, T., & Ittekkot, V. (2005). Nitrogen deficits in the Arabian Sea, implications from a three component mixing analysis. *Deep-Sea Research Part II Topical Studies in Oceanography*, *52*(14–15), 1879–1891. https://doi.org/10.1016/j.dsr2.2005.06.007

Ruddick, B. (1983). NOTE A practical indicator of the stability of the water column to double-diffusive activity. *Deep-Sea Research, Part A: Oceanographic Research Papers*, *30*(10A), 1105–1107. https://doi.org/10.1016/0198-0149(83)90063-8

Sastry, J., Premchand, K., & Murty, C. (1986). Watermass structure in the Western Indian Ocean : Part I-watermasses and their thermohaline indices. *Mausam*, *37*(1), 107–110. https://doi.org/10.54302/mausam.v37i1.2186

Schmidt, H., Czeschel, R., & Visbeck, M. (2020). Seasonal variability of the Arabian Sea intermediate circulation and its impact on seasonal changes of the upper oxygen minimum zone. *Ocean Science*, *16*(6), 1459–1474. https://doi.org/10.5194/os-16-1459-2020

Schmidt, H., Getzlaff, J., Löptien, U., & Oschlies, A. (2021). Causes of uncertainties in the representation of the Arabian Sea oxygen minimum zone in CMIP5 models. *Ocean Science*, *17*(5), 1303–1320. https://doi.org/10.5194/os-17-1303-2021

Sheehan, P. M. F., Webber, B. G. M., Sanchez-Franks, A., Matthews, A. J., Heywood, K. J., & Vinayachandran, P. N. (2020). Injection of oxygenated Persian Gulf Water into the southern Bay of Bengal. *Geophysical Research Letters*, *47*(14). https://doi.org/10.1029/2020GL087773

Stramma, L., Schmidtko, S., Levin, L. A., & Johnson, G. C. (2010). Ocean oxygen minima expansions and their biological impacts. *Deep-Sea Research Part I Oceanographic Research Papers*, *57*(4), 587–595. https://doi.org/10.1016/j.dsr.2010.01.005

Swift, S. A., & Bower, A. S. (2003). Formation and circulation of dense water in the Persian/Arabian Gulf. *Journal of Geophysical Research*, *108*(1). https://doi.org/10.1029/2002jc001360

Turner, J. S. (1967). Salt fingers across a density interface. *Deep-Sea Research and Oceanographic Abstracts*, *14*(5), 599–611. https://doi.org/10.1016/0011-7471(67)90066-6

Vic, C., Roullet, G., Capet, X., Carton, X., Molemaker, M. J., & Gula, J. (2015). Eddy-topography interactions and the fate of the Persian Gulf Outflow. *Journal of Geophysical Research: Oceans*, *120*(10), 6700–6717. https://doi.org/10.1002/2015JC011033

Yang, W., Wei, H., Liu, Z., & Zhao, L. (2023). Widespread intensified pycnocline turbulence in the summer stratified Yellow Sea. *Journal of Geophysical Research: Oceans*, *128*(1). https://doi.org/10.1029/2022JC019023

Yao, F., & Johns, W. E. (2010). A HYCOM modeling study of the Persian Gulf: 2. Formation and export of Persian Gulf Water. *Journal of Geophysical Research: Oceans*, *115*(11). https://doi.org/10.1029/2009JC005788

You, Y. (2002). A global ocean climatological atlas of the Turner angle: Implications for double-diffusion and water-mass structure. *Deep-Sea Research I*, *49*(11), 2075–2093. https://doi.org/10.1016/S0967-0637(02)00099-7